

Modelling spectral line profiles of wind-wind shock emissions from massive binary systems

D. Falceta-Gonçalves, Z. Abraham & V. Jatenco-Pereira

Instituto Astronômico e Geofísico - University of São Paulo

Abstract

One of the most intriguing spectral features of WR binary stars is the presence of time-dependent line profiles. Long term observations of several systems revealed the periodicity of this variability, synchronized with the orbital movement. Several partially successful models have been proposed to reproduce the observed data. The most promising assume that the origin of the emission is the wind-wind interaction zone. In this scenario, two high velocity and dense winds produce a strong shock layer, responsible for most of the X-rays observed from these systems. As the gas cools down, flowing along the interaction surface, it reaches recombination temperatures and generates the emission lines. Luhrs (1997) noticed that, as the secondary star moves along its orbital path, the shock region, of conical shape, changes its position with relation to the line of sight. As a consequence, the stream measured Doppler shift presents time variations resulting in position changes of the spectral line. However, his model requires a very thick contact layer and also fails to reproduce recently observed line profiles of several other WR binary systems. In our work, we present an alternative model, introducing turbulence in the shock layer to account for the line broadening and opacity effects for the asymmetry in the line profiles. We showed that the gas turbulence avoids the need of an unnaturally large contact layer thickness to reproduce line broadening. Also, we demonstrated that if the post-shock gas is optically thick at the observed line frequency, the emission from the opposing cone surface is absorbed, resulting in a single peaked profile. This result fully satisfy the recent data obtained from massive binary systems, and can help on the determination of both winds and orbital parameters. We succesfully applied this model to the Br22 system and determined its orbital parameters.

0.1 Introduction

WR and O stars present mass-loss rates of $\dot{M} \simeq 5 \times 10^{-5} - 10^{-7} M_{\odot} \text{ yr}^{-1}$ and wind velocities of $v \simeq 2000 - 3000 \text{ km s}^{-1}$ (Abbott et al. 1986, Willis 1991, Lamers & Leitherer 1993, Lamers 2001). In massive binary systems, the dense and supersonic winds produce a contact surface between two shock fronts along which the continuously incoming material flows. The shocked gas is characterized by high densities and temperatures, the latter reaching up to $T = 10^6 - 10^8 \text{ K}$.

The shock region is detectable directly, by free-free continuum and line emission from radio wavelengths to X-rays (Williams et al. 1990, Pittard et al. 1998, Bartzakos, Moffat & Niemela 2001, Abraham et al. 2005), and indirectly by IR emission from dust formed at the contact surface (Monnier, Tuthill & Danchi 2001, Falceta-Gonçalves, Jatenco-Pereira & Abraham 2005).

Isolated hot stars present broadened emission lines with variability in both amplitude and profile, which are usually attributed to the clumpiness of the stellar winds (Lèpine & Moffat 1999, Lèpine et al. 2000). However, in binary systems, the origin of the variability must be related to the binary system properties, since the observed line profiles repeat each orbital cycle (Seggewiss 1974). Luhrs (1997) proposed a purely geometrical model in which the observed spectrum was a composition of the stellar and the shocked gas emissions. This model was quite successfully applied to WR 79, showing itself very useful for the determination of the orbital parameters, as period and eccentricity, as well as stellar wind velocities and mass loss rates. However, Hill et al. (2000) and Bartzakos, Moffat & Niemela (2001) showed that the model was not able to fully reproduce the line profiles of several other WR binary systems.

In this work, we present a similar but improved model, in which we also assume that the lines are produced in the post-shock gas, but their profiles are affected by turbulence and opacity in the contact surface, which change at each point of the binary orbit. In section 2 we describe the model geometry and flux calculation, in section 3 we present the results obtained for different stellar and orbital parameters, followed by the conclusions in section 4.

0.2 The Line Profile Model

To model the line profile it is necessary to determine the relationship between the line intensity and the observed velocity. Since we assume that the line is produced in the shocked region, it is necessary to know the temperature structure and gas flow velocity along the contact surface projected into the line of sight for each orbital phase. We will present next a simplified model for the shock geometry and discuss latter the calculation method for the line profile including turbulence and opacity.

0.2.1 The geometry

When the two winds collide, an interaction zone is created that consists of two shock fronts at both sides of a contact surface. At the shock fronts, the temperature of the gas is highly increased, reaching up to $10^5 - 10^8$ K, depending on the wind velocities. The densities are also higher in the interaction zone. For adiabatic supersonic shocks, the density increases by a factor ~ 4 , but if radiative cooling is efficient, this factor may be much larger.

The contact surface is defined as the region where the momentum balance between the two winds occurs. Luo, McCray & Mac-Low (1990) and Stevens, Blondin & Pollock (1992) presented an analytical equation for its geometry, given by:

$$\frac{dy}{dz} = \frac{(\eta^{-1/2}d_2^2 + d_1^2)y}{\eta^{-1/2}d_2^2z + d_1^2(z - D)}, \quad (1)$$

where D is the distance between the stars; d_1 and d_2 are the distances of the primary and secondary stars to the contact surface, respectively, and $\eta = \dot{M}_s v_s / \dot{M}_p v_p$, where \dot{M}_p and \dot{M}_s are the mass loss rates of primary and the secondary stars, and v_p and v_s their respective wind velocities.

Asymptotically, this surface becomes conical, with an opening angle β . In Figure 1 (left panel) we show the contact surface (S_C) given by Equation 1, for $\eta = 0.1$ that corresponds to $\beta \simeq 44^\circ$; the two shock fronts S_1 and S_2 are also schematically represented. For certain recombination lines (e.g. UV and visible) we expect the major emission to come from larger distances of the shock apex, where the gas has cooled. In this case, we will assume the conical geometry in the further calculations.

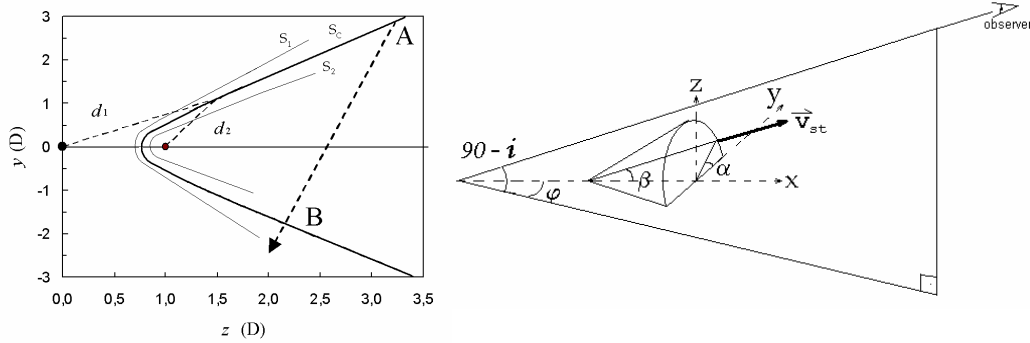


Figure 1: Left: Momentum balance surfaces of the colliding winds for both $\eta = 0.1$ which result in $\beta = 44^\circ$. The dots represent each star, and the arrow represents the line of sight intercepting the points labeled A and B (see Section 2.3). Right: Schematic view of the assumed geometry.

We will assume that all the physical parameters of the shock gas are cylindrically symmetric with respect to the cone axis and that the stream velocity is constant along the contact surface. As we will see later, with these assumptions it is not necessary to know the exact temperature and density distributions of the shocked material to calculate the normalized line profiles.

To calculate the stream velocity projected into the line of sight we use the schematic geometry shown in the right panel of Figure 1. We define the x axis by the straight line containing both stars and, as a consequence, coincident to the cone symmetry axis. Notice that this is correct if inertial deformations due to the orbital motion of the secondary star are neglected. We will discuss later the main effects of this deformation in the obtained results. The y axis, together with x , defines the orbital plane.

The stream velocity projected over the line of sight, as shown in Figure 1, is given by:

$$v_{\text{obs}} = v_{\text{flow}}(-\cos \beta \cos \varphi \sin i + \sin \beta \cos \alpha \sin \varphi \sin i - \sin \beta \sin \alpha \cos i), \quad (2)$$

where v_{flow} is the stream velocity, i is the inclination of the orbital plane with respect to the line of sight, α is the cone azimuthal angle and φ is the orbital

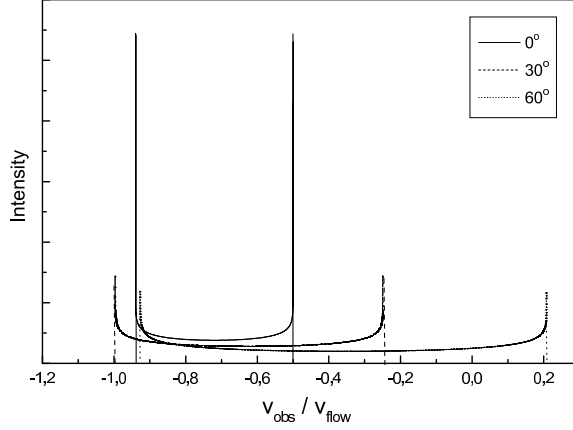


Figure 2: Synthetic line profiles, obtained from Equations 2 - 4 for orbital phases ranging from 0° to 180° , assuming $i = 70^\circ$ and $\beta = 40^\circ$.

phase, defined here as the angle between x and the projection of the line of sight on the orbital plane.

Equation 2 shows that, for a given orbital phase φ , each fluid element with a different α value will contribute with a different Doppler shift.

Assuming azimuthal symmetry for the gas properties over the cone surface, the line intensity distribution $I(\alpha)$ originated by a volume element at azimuth α will be:

$$I(\alpha) = \frac{I}{2\pi}, \quad (3)$$

where I is the total line intensity. The line profile distribution $I(v_{\text{obs}})$ can be obtained from the relation:

$$I(\alpha)d\alpha = I(v_{\text{obs}})dv_{\text{obs}}. \quad (4)$$

Substituting $dv_{\text{obs}}/d\alpha$, given by Equation 2 into Equation 4, the line profile can be determined. In Figure 2 we show the calculated synthetic line profiles for different values of the orbital phase, assuming $i = 70^\circ$ and $\beta = 40^\circ$.

0.2.2 Line Broadening

The profiles shown in Figure 2 are unable to reproduce the observations because they are discontinuous and present large differences between the peak and the lower emission intensities. The introduction of some sort of broadening could reduce the discrepancy.

Luhrs (1997) noticed from numerical simulations of adiabatic shocks that the emitting region is delimited by two conic surfaces with $\beta_1 < \beta < \beta_2$. Using an *ad hoc* flux density distribution over β he obtained broadened synthetic line profiles. Varying $\Delta\beta = \beta_2 - \beta_1$ between 37° and 54° , depending on the orbital phase, he was able to fit for WR79 the observed CIII 5696Å lines at some orbital phases, but failed to reproduce others. Besides, in massive binary systems, the shock is highly radiative because of the high density at the contact surface, resulting in thin and turbulent layers (Stevens, Blondin & Pollock 1992). For that reason, $\Delta\beta$ is expected to be lower near periastron, as the density is higher, in disagreement to the hypothesis used by Luhrs (1997). The variable $\Delta\beta$ model also failed to reproduce the line profiles of other WR binary systems (Hill, Moffat, St-Louis & Bartzakos 2000, Bartzakos, Moffat & Niemela 2001).

Since the numerical models mentioned above predict the existence of a highly turbulent contact surface, in the present work we introduced turbulence in the calculation of the line profile, using a constant single value for the β parameter. For that, we assumed that each emitting element at a given α has a gaussian velocity distribution, with a mean value obtained from Equation 2, and a dispersion amplitude σ . Therefore, different emitting elements, at different α values may present the same observed velocity. In this case, since there is no univocal relationship between the velocity projected into the line of sight and α , Equation 4 is no longer valid and the line profile must be obtained from:

$$I(v) = \mathcal{C} \int_0^\pi \exp \left[-\frac{(v - v_{\text{obs}})^2}{2\sigma^2} \right] d\alpha, \quad (5)$$

where \mathcal{C} is the normalization constant. Substituting the mean value v_{obs} , given by Equation 2, and integrating the right hand side of the equation over α , we obtain the relative line intensity for each projected velocity into the line of sight v .

0.2.3 Opacity Effects

Bartzakos, Moffat and Niemela (2001) obtained the spectra of Br22 (WC4), a binary system in the Magellanic Clouds, at several epochs. They found that the CIII 5969Å line could be explained by a superposition of a constant feature and an emission excess that varied across the line profile according to the orbital phase. In contrast to what is expected for binary systems from the Luhrs model, these excesses were single peaked. Norci et al. (2002) observed the same behavior for several other Galactic WR stars.

A possible explanation for the single peaked profiles could be the enhanced absorption of some of the emission by the dense gas layer at the contact surface, when positioned in front of it. In fact, the density of the interaction zone depends on the stellar mass-loss rates and on the separation between the stars, and could eventually become high enough to absorb part of the incoming photons (Falceta-Gonçalves, Jatenco-Pereira & Abraham 2005).

In Figure 1 (left panel), we illustrate a given situation in which the line of sight (dashed arrow) intercepts the regions of the contact surface labeled A and B. As the cone is intercepted by the line of sight, the emission element A, responsible for the “redder” peak of the synthetic profile, could be obscured by the absorbing element B. The opacity of this element is unknown, since it depends both on the undetermined gas density and temperature. However, if the cooling process is effective, the gas will reach high densities as the temperature diminishes, becoming eventually optically thick for certain wavelengths. This is expected to occur mainly in close massive binary systems.

In this work we introduced an optical depth τ into Equation 5. For a given orbital phase, when two emitting fluid elements are intercepted by the line of sight, the observed emission from the farthest element will be diminished by a factor $\exp(-\tau)$ while the emission from the nearest will remain unchanged. If $\tau \gg 1$, we could obtain a single peaked line profile. Actually, a more detailed model solving the complete radiative transfer equations would result in a lower relative intensity for the intervening material emission. However, the qualitative result for $\tau \gg 1$ remains the same, and for $\tau < 1$ no important changes occurs.

Since the opacity of the contact surface depends on the separation between the stars, the interaction region of close binary systems could be optically thick while systems with large separations could be optically thin. That explains why certain systems present a single peak in their spectra during all

the orbital period, while others present double peaked profiles.

0.3 Results and Discussion

We will investigate the effects of the binary system parameters on the line profiles, using the model described in section 2. Initially, we will neglect opacity, *i.e.* use $\tau = 0$, fix $\beta = 40^\circ$ and a low turbulence amplitude $\sigma/v_{\text{flow}} = 0.05$, varying the orbital inclination i . In Figure 3 we present the normalized line intensity profiles, in arbitrary units, for $i = 90^\circ$ (top), 70° (middle) and 20° (bottom), at different orbital phases from $\varphi = 0^\circ$ to 180° . For $i = 90^\circ$, at $\varphi = 0^\circ$, the cone is pointed directly towards the observer with all emitting gas being observed with the same mean velocity, resulting in a strong peak with mean velocity given by the first term of Equation 2. The highest Doppler shift occurs when $\varphi = \beta$ and $\varphi = 180^\circ - \beta$, as the line of sight coincides with the cone generatrix. Also, it is noticeable that the line profiles present larger variation during the orbital period for larger values of i . For face-on oriented systems, the observed line will not show any variation during the orbital period.

In Figure 4 we show the effects of the cone opening angle on the line profiles. Here we neglected absorption, fixed $i = 70^\circ$ and $\sigma/v_{\text{flow}} = 0.05$, and compared the results for $\beta = 40^\circ$ (top) and 70° (bottom) at different orbital phases. The main difference occurs on the distance between the peaks. The larger the opening angle the larger is the peak separation. It shows that, for a given system in which both peaks are detectable during all orbital phases, it is possible to determine β , *i.e.* the relation between the stellar wind momenta.

The stream turbulence also play an important role in the emission line profiles. In Figure 5, we neglected absorption, fixed $i = 70^\circ$ and $\beta = 40^\circ$, and obtained the results for the turbulence amplitudes $\sigma/v_{\text{flow}} = 0.05$ (top) and 0.20 (bottom) at different orbital phases. Obviously, by increasing the flow turbulence at the post-shock region we obtained broadened line profiles, as in Luhrs (1997). However, in this case, it was not necessary to use a high and unrealistic difference between the internal and external cone opening angles. A high turbulent system may, eventually, show a plateau instead of a two peaked profile as both peaks tend to merge. This would be an indication of a strongly radiative shock.

Finally, in Figure 6 we simulate a strong absorption during the synthetic line profile computation. For that, we fixed $i = 90^\circ$, $\beta = 40^\circ$ and $\sigma/v_{\text{flow}} =$

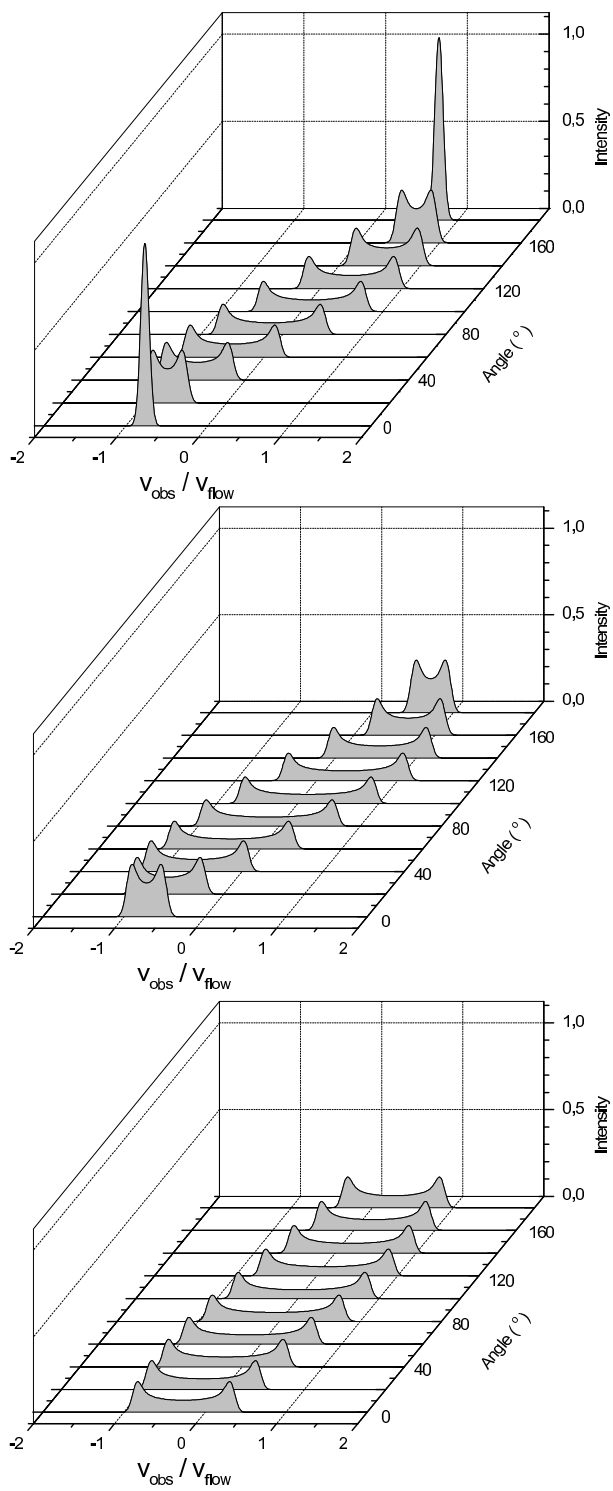


Figure 3: Theoretical line profiles considering $\sigma/v_{\text{flow}} = 0.05$ and $\beta = 40^\circ$ for $i = 90^\circ$ (top), 70° (middle) and 20° (bottom), neglecting absorption.

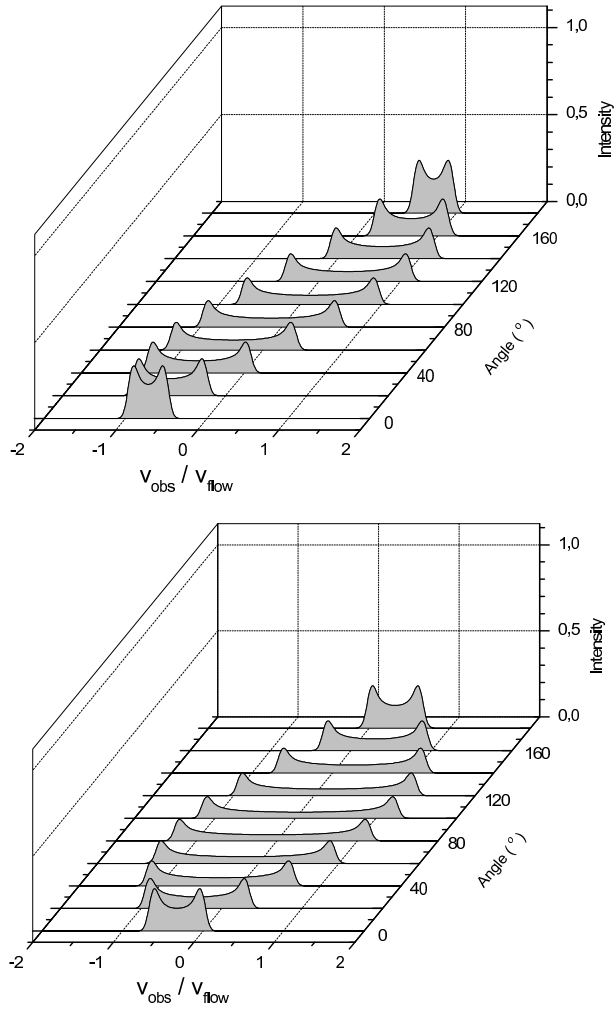


Figure 4: Theoretical line profiles considering $i = 70^\circ$ and $\sigma/v_{\text{flow}} = 0.05$ for $\beta = 40^\circ$ (top) and 70° (bottom), neglecting absorption.

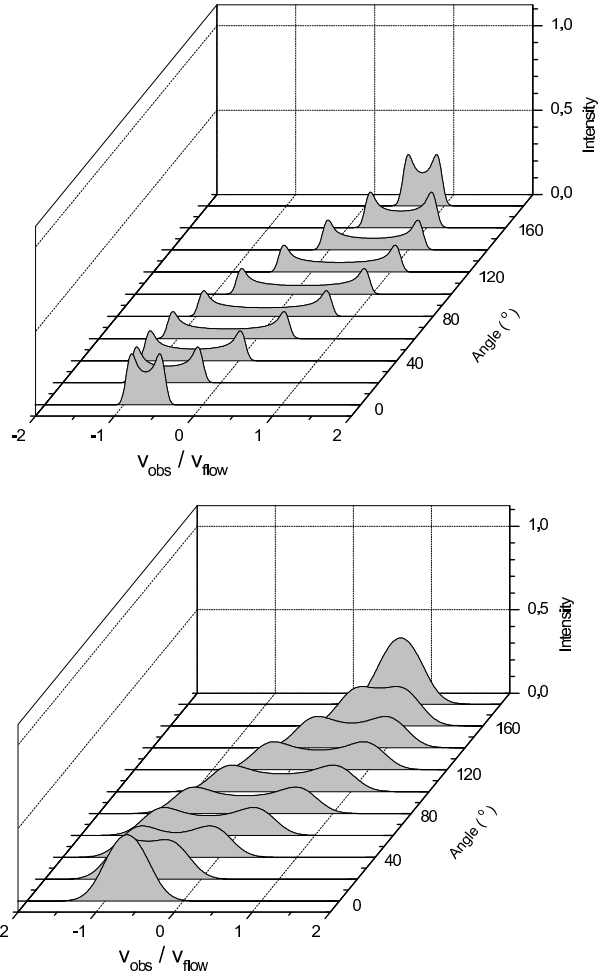


Figure 5: Theoretical line profiles considering $i = 70^\circ$ and $\beta = 40^\circ$ for $\sigma/v_{\text{flow}} = 0.05$ (top) and 0.20 (bottom), neglecting absorption.

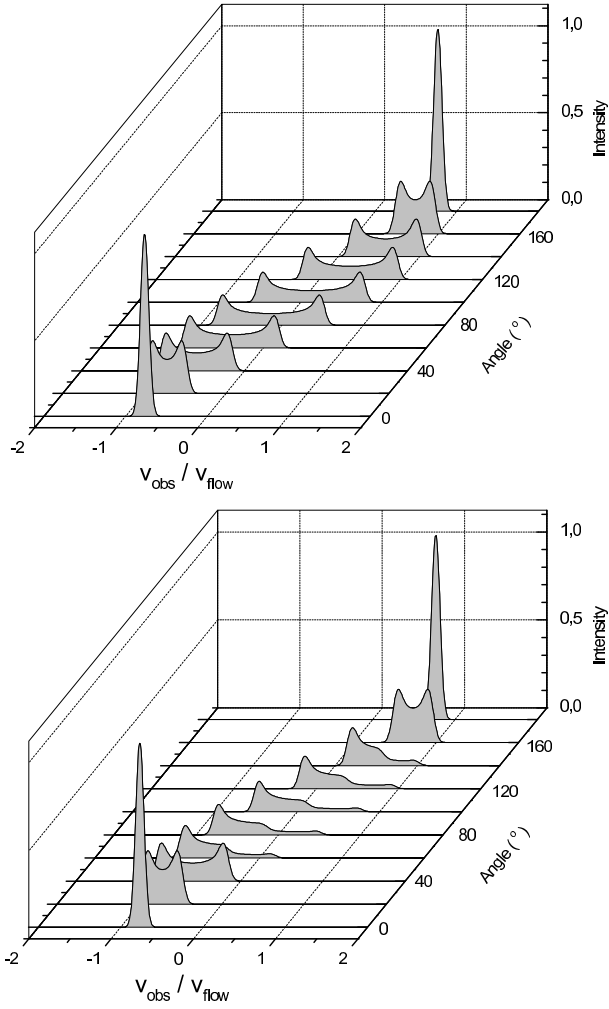


Figure 6: Theoretical line profiles considering $\sigma/v_{\text{flow}} = 0.05$, $\beta = 40^\circ$ and $i = 90^\circ$ for $\tau = 0$ (top) and $\tau \gg 1$ (bottom).

0.05, and performed the calculations for $\tau = 0$ (top) and $\tau \gg 1$ (bottom) at different orbital phases. In this case, the main difference in the line profile occurs at the orbital phases $\beta < \varphi < 180^\circ - \beta$, in which the redder part of the profile is absorbed, resulting in a single peaked profile. For face-on systems ($i = 0^\circ$), the single peak feature occurs during the entire orbital period. Also, an interesting fact is that the blueshifted peak will be unabsorbed, while the redshifted may be totally absent. Qualitatively, this result is in full agreement with the observations of several binary systems that were not reproduced by the Luhrs synthetic profiles (Bartzakos, Moffat and Niemela 2001, Norci et al. 2002).

0.3.1 The case of Br22

Br22 (HD 35517), a massive WR+O binary system located in the Large Magellanic Cloud, presents periodic line profile variations. The CIII 5696 Å emission line is probably produced at the shock site and can provide clues on the wind and orbital parameters. Bartzakos, Moffat & Niemela (2001) applied Luhrs model to this object, obtaining a best fit for $i = 30^\circ$, $v_{flow} = 2700 \text{ km s}^{-1}$ and $\Delta\beta = 45^\circ$. However, photometric, spectrometric and polarimetric studies determined the actual orbital inclination as $i \sim 70^\circ$; and peak position analysis gave a direct estimate for the stream mean velocity $v_{flow} \sim 1500 \text{ km s}^{-1}$. Also, qualitatively, the observed peak relative intensities are in disagreement to the synthetic lines. These discrepancies show that the Luhrs profiles are not able to reproduce these observations.

We applied the model described in this work for the Br22 system fixing $i = 71^\circ$, $v_{flow} \sim 1500 \text{ km s}^{-1}$ and $\beta = 47^\circ$, as determined by the observations. Then, we varied the turbulence amplitude and the opacity in order to obtain the best fitting to the observed profiles (Figure 5 of Bartzakos, Moffat & Niemela 2001). This result, corresponding to $\sigma/v_{flow} = 0.25$ and $\tau = 0.6$, is shown in Figure 7, where the light and dark lines correspond to the synthetic and the observed profiles, respectively. As explained above, since the two peaks are marginally detected from the observations, the value of τ must be lower than unity, as determined by the best fitting.

As we can see, the synthetic profiles match quite well both the bulk profile and the peak positions. Although considerably better than the Luhrs model adjusts, the bottom spectra of Figure 7 show broader observed lines. Actually, there is some difficulties on separating the emission lines from the continuum, and better fittings could be obtained depending on the data

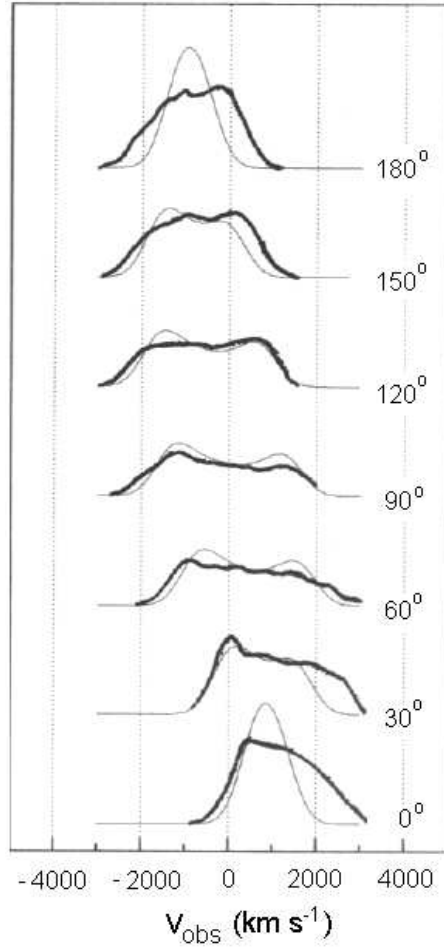


Figure 7: Model application for Br22 assuming $i = 71^\circ$, $v_{flow} = 1500 \text{ km s}^{-1}$ and $\beta = 47^\circ$ (Bartzakos, Moffat & Niemela 2001), and adjusting $\sigma/v_{flow} = 0.25$ and $\tau = 0.6$.

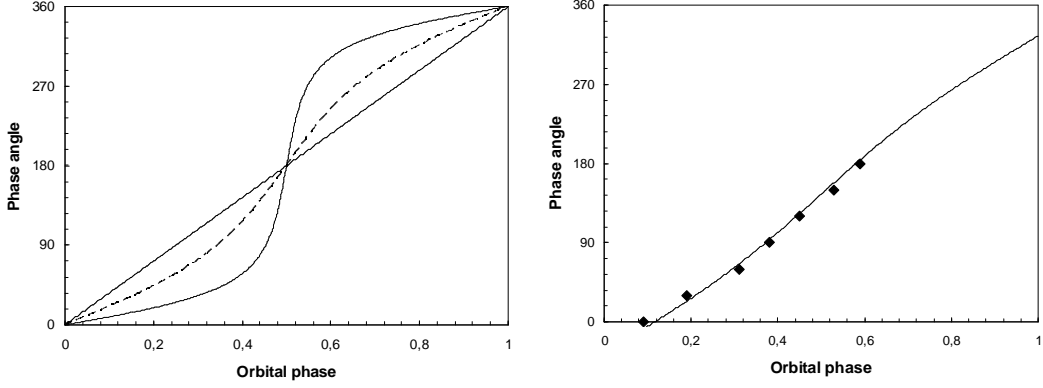


Figure 8: Left: The dependence of the phase angle on the orbital phase for eccentricities $e = 0.0$ (solid), 0.3 (dashed) and 0.7 (dotted). Right: the phase angle variation, obtained from Figure 7, for Br22 and the best fit for $\varphi_0 = 35^\circ$ and $e = 0.1$.

baseline subtraction. If real, these differences can be explained if, instead of a perfect cone, the shock surface is curved by the stellar orbital motion. In this scenario, the emission would not be concentrated to form the two peaked profile, but distributed over the possible radial velocities. Also, we assumed that the flow velocity is constant during the orbital period what is not necessarily true. Higher eccentric orbits would lead to different flow velocities, and different shock turbulence, as the stars move along their orbits. These hypothesis could be verified using time-dependent numerical simulations.

In addition to the turbulence and opacity derived from our model, we were able to constrain some of the orbital parameters. To do that, for each orbital phase obtained from the observations, we determined the corresponding model phase angle, which depends on the eccentricity (e) and the angle between the semi-major axis and the line of sight (φ_0), by comparing the shape of the line profile and the peak position. The results of our best fitting are $e = 0.1$ and $\varphi_0 = 35^\circ$; in Figure 8 we show the dependence of the phase angle on the orbital phase for three values for the eccentricity (left panel) and the best fit to the observation (right panel).

0.4 Conclusions

In this work we present a model to explain the variable line emission profiles of WR binary stars. Following Luhrs (1997), we assumed that the observed emission lines are formed at the wind-wind interaction zone by the cooling gas flowing along the contact surface. Besides, we introduced turbulence as a new parameter and also studied the effects of the shock layer opacity on the synthetic line profiles.

Our model recovered the standard result of two peaked profiles, and their dependence on the orbital plane inclination and on the cone opening angle. However, the line broadening is assumed to be the consequence of a highly turbulent environment in strongly cooling shocks. In this case, it is not necessary to assume unreal large shock layer widths to reproduce the observations. We also showed that the opacity is responsible for the intensity reduction of the reddened peak. In this sense, a highly opaque post-shock gas results in a line profile with a single blue-shifted peak, as occurs for some observed systems.

In particular we applied this model to Br22 and were able to reproduce fairly well the line profiles for the different orbital phases using the observed parameters $i = 71^\circ$, $v_{flow} \sim 1500 \text{ km s}^{-1}$ and $\beta = 47^\circ$ and assuming $\sigma/v_{flow} = 0.25$ and $\tau = 0.6$. By comparing the observed and model profiles we were also able to determine the eccentricity and the angle between the periastron and the line of sight ($e = 0.1$ and $\varphi_0 = 35^\circ$).

We did not take into account the inertial effect of the secondary motion on the cone geometry deformation. A direct effect is the variation on the angle between the cone axis and the line of sight. However, we performed our calculations in terms of φ , which exactly corresponds to this parameter and not strictly the orbital phase. Actually, to obtain the orbital phase it is necessary to subtract (or add) the angle variation ($\delta\varphi$) to φ . The other effect of the stellar motion is the curvature of the cone generatrix. As discussed above, in the case of very close binaries, this curvature could be high enough to flatten the observed profile. We also did not take into account the possible phase-dependent variations of the flow velocity and shock turbulence, as could occur in high eccentric orbits. Numerical simulations are needed to quantify these effects.

Acknowledgments

D.F.G thanks FAPESP (No. 04/12053-2) for financial support. Z.A. and V.J.P. thank FAPESP, CNPq and FINEP for support.

References

- Abbott, D. C., Biegging, J. H., Churchwell, E. & Torres, A. V. 1986, *ApJ*, 303, 239.
- Abraham, Z., Falceta-Gongalves, D., Dominici, T. et al. 2005, *MNRAS*, 364, 922.
- Bartzakos, P., Moffat, A. F. J. & Niemela, V. S. 2001, *MNRAS*, 324, 33.
- Davidson, K., Martin, J. C., Humphreys, R. M. & Ishibashi, K. 2005, *AAS*, 206, 808.
- Falceta-Gongalves, D., Jatenco-Pereira, V. & Abraham, Z. 2005, *MNRAS*, 357, 895.
- Henley, D. B., Stevens, I. R. & Pittard, J. M. 2003, *MNRAS*, 346, 773.
- Hill, G. M., Moffat, A. F. J., St-Louis, N. & Bartzakos, P. 2000, *MNRAS*, 318, 402.
- Hummer, D. G. & Storey, P. J. 1987, *MNRAS*, 224, 801.
- Lamers, H. J. G. L. M. & Leitherer, C. 1993, *ApJ*, 412, 771.
- Lamers, H. J. G. L. M. 2001, *PASP*, 113, 263.
- Lèpine, S. & Moffat, A. F. J. 1999, *ApJ*, 514, 909.
- Lèpine, S., Moffat, A. F. J., St. Louis, N., Marchenko, S. V. et al. 2000, *AJ*, 120, 3201.
- Luhrs, S. 1997, *PASP*, 109, 504.
- Luo, D., McCray, R. & Mac-Low, M. 1990, *ApJ*, 362, 267.
- Monnier, J., Tuthill, P. & Danchi, W. 2001, *A&AS*, 199, 608.
- Norci, L., Viotti, R. F., Polcaro, V. F. & Rossi, C. 2002, *RMxAA*, 38, 83.
- Pittard, J. M., Stevens, I. R., Corcoran, M. F. & Ishibashi, K. 1998, *MNRAS*, 299, 5.
- Seggewiss, W. 1974, *A&A*, 31, 211.
- Stevens, I. R., Blondin, J. M. & Pollock, A. M. T. 1992, *ApJ*, 386, 265.
- Williams, P. M., van der Hucht, K. A., Pollock, A. M. T. et al. 1990, *MNRAS*, 243, 662.
- Willis, A. J. 1991, *Proc. IAU 143*, Wolf-Rayet Stars: and interrelations with other massive stars in galaxies, ed. K. A. van der Hucht and B. Hidayat

(Dordrecht, Kluwer), p265.